Identifying grey-box models from archetypes of apartment block buildings

Marius Bagle[1], Phillip Maree[2], Harald Taxt Walnum[1], Igor Sartori[1]
[1]SINTEF Community, Oslo, Norway
[2]SINTEF Digital, Trondheim, Norway

Abstract

Advanced building control strategies, like Model Predictive Control, has thus far seen limited implementation in real buildings. A key challenge to overcome is the development of robust methods for model identification. Although much work has been done in the way of mathematical methods for generating models, the practical applications are still in the early stages. In particular, most model identification methods require high-quality data, usually only obtained in an experimental setting. In this work, a method to short-circuit this process by using validated simulation models to obtain suitable grey-box models is developed, by leveraging existing software. The resulting models show consistent although time-varying dynamics, in addition to reasonable simulation performance under a variety of conditions.

Key Innovations

- Procedure for generating grey-box models for aggregated dynamics of simulation models.
- Consistent parameter estimates across months and seasons, reasonable simulation performance.

Practical Implications

Under certain conditions, grey-box models can replace white-box simulation models. However, beware of nonphysical parameters.

Introduction

Energy use in buildings constitute approximately 40 % of the final energy use (a large portion of which goes toward heating, cooling, ventilation and air-conditioning) and 36 % of greenhouse gas emissions in Europe (European Commission, 2019). To enable a decarbonization of the energy system and reach the 2 degree goal (UN, 2020), a comprehensive phase-in of renewable energy sources must be undertaken. Since the potential of stable sources such as geothermal and hydro-power is limited, a large share must come from wind and solar power. The inherent intermittency of these sources leads to new challenges in how energy and power systems are operated, and traditional central load-matching will become insufficient as the penetration of these sources increase. A key concept in this context is energy flexibility on the demand side (i.e. in buildings, either residential or commercial), enabling the grid/system operator to control the demand through penalty signals, associated with e.g. price, CO2-emissions and grid congestion (Junker et al., 2018). Model Predictive Control (MPC) is regarded as an important enabling technology for the activation of this flexibility (in other words, an ability to respond to the price signals must exist on the receiving end). MPC is a well-established control strategy for constrained optimization which enables energy flexibility by exploiting energy storage capabilities and optimization of renewable on-site generation. In addition, incorporation of forecast models (i.e., internal gains, weather), and given user inputs (e.g. comfort ranges, electric vehicle charging needs) allows anticipation of energy needs which can be optimized for flexible energy sources (Serale et al., 2018). Despite the prevalent success of MPC within the process industry (Qin and Badgwell, 2003), the practical implementation thereof in buildings has predominantly been slowed due to (1) required controller model development and estimation of unknown states (Cígler et al. (2013), Blum et al. (2019)); (2) lack of operational knowledge among building management system engineers w.r.t modern optimal control methods (Drgoňa et al., 2020).

A common conceptual approach is to use reduced-order models based on simple physics, combined with data-driven inference of the parameters, so-called *grey-box* models (Bacher and Madsen (2011), Coninck et al. (2016)). However, open research questions remain in this field. For instance, most efforts to identify models treat the process as a one-time effort, when in reality, it is uncertain whether one model can cover all operating and weather conditions. Furthermore, the large variance in the built environment means that the model identification process must be done for each building on which MPC is to be implemented (Blum et al., 2019). This paper shows a method for generating "initial" control-models (parameter bounds) for an iterative online estimation strategy, such as is outlined in e.g. (Maree et al., 2021), at scale.

Another motivation for developing grey-box models at scale is their potential use in large-scale flexibility studies, i.e. investigating the theoretical potential of implementing a control strategies, such as MPC, at

several hierarchy levels of the energy system. Such studies are present in the literature, but employ either white-box simulation models (Majdalani et al., 2020), or an implicit representation of the indoor temperature (Romanchenko et al., 2018).

Methods

In this section, relevant background theory will be presented, along with a description of the dataset and the simulation model used. Furthermore, the full model deployed in the "batch estimation" procedure will be presented, along with the algorithm for the procedure.

Maximum Likelihood Estimation

The aim is the model/system identification procedure is to find the parameters $\boldsymbol{\theta}$ that maximize the likelihood of a sequence of measurements. For k measurements taken from time $t = 0$ to $t = k$, henceforth denoted t_k, we define the measurement vector $\mathcal{Y}_k$, where

$$\mathcal{Y}_k = [\boldsymbol{y}_k, \boldsymbol{y}_{k-1}, ..., \boldsymbol{y}_1, \boldsymbol{y}_0] \tag{1}$$

The likelihood of the full series of measurements $\mathcal{Y}_N$ given the parameters $\boldsymbol{\theta}$ is the joint probability density:

$$L(\boldsymbol{\theta}; \mathcal{Y}_N) = p(\mathcal{Y}_N|\boldsymbol{\theta}) \tag{2}$$

which can be stated equivalently:

$$L(\boldsymbol{\theta}; \mathcal{Y}_N) = \left(\prod_{k=1}^{N} p(\boldsymbol{y}_k|\mathcal{Y}_{k-1}, \boldsymbol{\theta} \right) p(\boldsymbol{y}_0|\boldsymbol{\theta}) \tag{3}$$

i.e. as a product of conditional probability densities. Because the evaluation of this equation is computationally infeasible in practice, a simpler method based on Kalman filtering is used instead. This can be done because the the diffusion/noise terms in equations 9 and 10 are assumed to be Wiener processes (which have Gaussian increments), which makes the assumption of Gaussian conditional densities at each time step reasonable. Since the Gaussian density is completely characterized by its mean and covariance, we can write the likelihood L as:

$$L(\boldsymbol{\theta}; \mathcal{Y}_N) = \left(\prod_{k=1}^{N} \frac{\exp(-\frac{1}{2}\boldsymbol{\epsilon}_k^T \boldsymbol{R}_{k|k-1}^{-1} \boldsymbol{\epsilon}_k)}{\sqrt{\det(\boldsymbol{R}_{k|k-1})}(\sqrt{2\pi})^l} \right) p(\boldsymbol{y}_0|\boldsymbol{\theta}) \tag{4}$$

where the notation:

$$\hat{\boldsymbol{y}}_{k|k-1} = E\{\boldsymbol{y}_k|\mathcal{Y}_{k-1}, \boldsymbol{\theta}\} \tag{5}$$

$$\boldsymbol{R}_{k|k-1} = V\{\boldsymbol{y}_k|\mathcal{Y}_{k-1}, \boldsymbol{\theta}\} \tag{6}$$

is used for the conditional mean E and variance V of $\boldsymbol{y}_k$, given the measurements up to t_{k-1} and the parameters $\boldsymbol{\theta}$. Furthermore, the residual ϵ is defined as:

$$\boldsymbol{\epsilon}_k = \boldsymbol{y}_k - \hat{\boldsymbol{y}}_{k|k-1} \tag{7}$$

i.e. as the difference between the actual measurement $\boldsymbol{y}_k$ and the *a priori* model estimate of $\boldsymbol{y}_k$, $\hat{\boldsymbol{y}}_{k|k-1}$, which is found via the equations of the Kalman filter (Kristensen and Madsen, 2003). The likelihood function is evaluated by computing 5 and 6 recursively with these equations. A quasi-Newton method is used to optimize the parameters $\boldsymbol{\theta}$ on top of this, such that the likelihood is maximized, i.e. the negative log-likelihood minimized. The optimization problem to be solved is:

$$\hat{\boldsymbol{\theta}} = \arg\min_{\boldsymbol{\theta} \in \Theta} \{-\ln(L(\boldsymbol{\theta}; \mathcal{Y}_N|\boldsymbol{y}_0))\} \tag{8}$$

where $\Theta \subset \mathbb{R}^p$ is the parameter space, possibly constrained above by $\boldsymbol{\theta}_{max}$ and below by $\boldsymbol{\theta}_{min}$. For the full mathematical treatment of the method used, see Kristensen and Madsen (2003).

Data

For the model identification process, datasets from IDA-ICE (Kalamees, 2004) simulations, using *archetype* (TABULA/EPISCOPE, 2013) models of Norwegian apartment blocks are used (Sartori and Rønneseth, 2018). Of a total 21 variations of the eight archetypes AB01 to AB08, eight variations of three archetypes have been simulated in IDA-ICE.

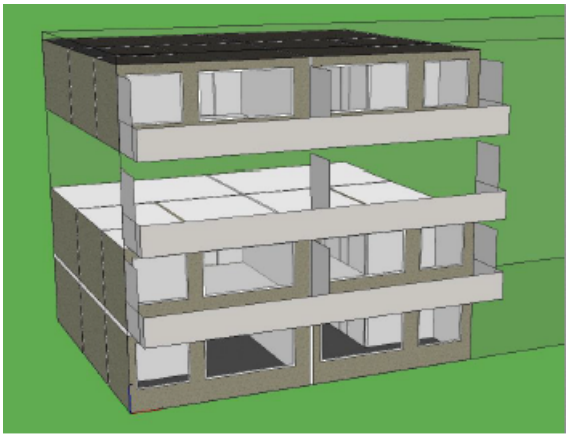

Figure 1: Visual of IDA-ICE model.

The IDA-ICE simulations are done for a Norwegian typical meteorological year (TMY) (Renné, 2016), with a Pseudo-random binary signal (PRBS) applied to the heating control system (Bottolfsen et al., 2020). The heating system is hydronic, with a plant-level central heater supplying radiators at the zone-level. The signal is applied from the 1^{st} to the 20^{th} in every month of the year, with the rest of the each month being *normal* operation, i.e. tracking a set-point with PI-controllers (at zone-level). One issue with the signal is that it is applied to the zone-level heaters in the IDA-ICE models, while a weather compensation curve modulating the supply temperature of the hydronic heating system remains. Thus, the signal is not a true PRBS, since the heating power has a certain dependency on the outdoor temperature. Figure 2 shows the extracted dataset for AB03 variant

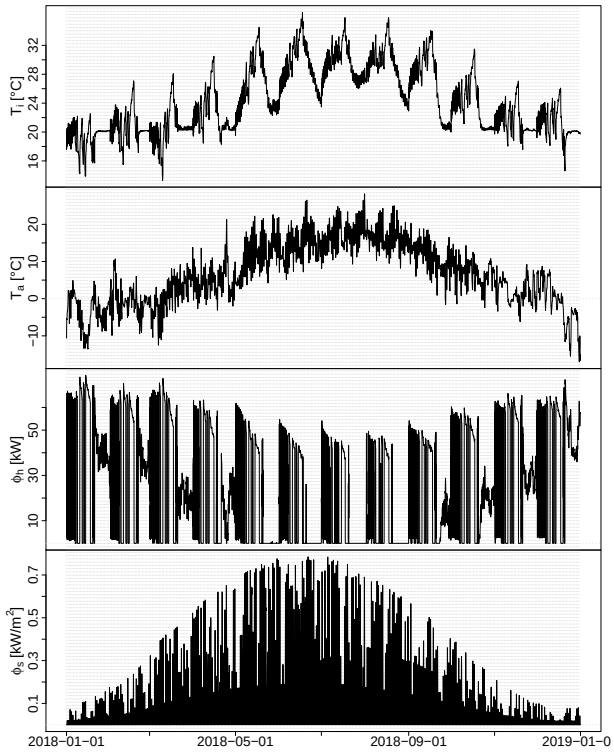

Figure 2: Dataset, AB03 Variant 2. Top to bottom: Indoor temperature, outdoor temperature, heating power, solar radiation.

2, where this modulation is visible. We see that the indoor temperature T_i is allowed to deviate substantially from normal comfort limits, ranging all the way from 13 °C to 35 °C, which should enable a sufficient excitation of the time constants in the system. Note that since we are dealing with aggregated models in this paper, the indoor temperature T_i is the average of all room temperatures, while the heating input ϕ_h is the plant-level heating power. The schedule for internal gains ϕ_int, although not shown here, is taken from the Norwegian standard for building simulation (Standards Norway, 2020). The sampling time T_s chosen for model identification procedure is one hour, as a higher sampling frequency would require upsampling the weather data (T_a, ϕ_s). Instead, indoor temperature T_i is sampled at a time instant (like a real temperature sensor), and the heating power ϕ_h is integrated (like a real energy meter) and averaged, both from a base sampling time of 5 minutes.

Model structure

In general, we are dealing with continuous-time linear stochastic grey-box models on the form (Kristensen and Madsen (2003)):

$$d\boldsymbol{x}_t = (\mathbf{A}(\boldsymbol{\theta})\boldsymbol{x}_t + \mathbf{B}(\boldsymbol{\theta})\boldsymbol{u}_t)dt + \boldsymbol{\sigma}(\boldsymbol{\theta})d\boldsymbol{\omega}_t \quad (9)$$

$$\boldsymbol{y}_k = \mathbf{C}(\boldsymbol{\theta})\boldsymbol{x}_k + \boldsymbol{e}_k \quad (10)$$

where $t \in \mathbb{R}$ is time, $\boldsymbol{x}_t \in \mathcal{X} \subset \mathbb{R}^n$ is a state vector, $\boldsymbol{u}_t \in \mathcal{U} \subset \mathbb{R}^m$ is an input vector, $\boldsymbol{y}_k \in \mathcal{Y} \subset \mathbb{R}^l$ is an output vector, $\boldsymbol{\theta}$ is as described in equation 8, $\mathbf{A}(\cdot) \in \mathbb{R}^{n\times n}$, $\sigma(\cdot) \in \mathbb{R}^{n\times n}$ and $\mathbf{C}(\cdot) \in \mathbb{R}^{l\times n}$ are non-linear functions (but as a function of only the parameters $\boldsymbol{\theta}$, they yield a linear system), $\{\boldsymbol{\omega}_t\}$ is an n-dimensional standard Wiener process, and $\{\boldsymbol{e}_t\}$ is an l-dimensional white-noise process, i.e. a linear time-invariant (LTI) model with no feed-forward from the input to the output.

An alternative formulation, which has the potential to better handle the non-linearities that arise on rapid switching events, is:

$$d\boldsymbol{x}_t = (\mathbf{A}(\boldsymbol{\theta})\boldsymbol{x}_t + \mathbf{B}(\boldsymbol{\theta})\boldsymbol{u}_t)dt + \boldsymbol{\sigma}(\boldsymbol{\theta}, \boldsymbol{u}'_t)d\boldsymbol{\omega}_t \quad (11)$$

where $\boldsymbol{u}'_t \in \mathcal{U}' \subset \mathbb{R}^{m+1}$ is an augmentation of the input vector $\boldsymbol{u}_t$ in 9 to include a lag on the heating input ϕ_h, defined as 1 up to t_{k+n} if $|\Delta\phi_\mathrm{h}|_k \leq 10$ from t_{k-1} to t_k and 0 otherwise.

In Bagle et al. (2020), the model $T_\mathrm{i}T_\mathrm{e}T_\mathrm{m}$ is found to be a sufficient model using the forward selection procedure described in Bacher and Madsen (2011), in addition to having the best validation performance. Ideally, a model that explicitly takes the thermal mass of the waterborne heating system into a account would be preferable. However, because the IDA-ICE models used as the basis for the model identification do not contain this, such models are discarded. Instead, we use the 3R3C-model $T_\mathrm{i}T_\mathrm{e}T_\mathrm{m}\sigma$ as the full model, with input dependent process noise/diffusion term denoted by σ. It can be represented by the circuit diagram in figure 3. The state equations can be written out explicitly by applying the node-voltage method (Kirchoffs current law) and adding process noise to each state:

$$\begin{aligned} dT_\mathrm{i} =& \frac{1}{R_\mathrm{ie}C_\mathrm{i}}(T_\mathrm{e} - T_\mathrm{i})dt + \frac{A_\mathrm{w}}{C_\mathrm{i}}\phi_\mathrm{s} + \frac{1}{C_\mathrm{i}}\phi_\mathrm{int} \\ &+ \frac{1}{C_\mathrm{i}}\phi_\mathrm{h} + (1 + Q_\mathrm{step}\sigma_\mathrm{level})\exp(\sigma_\mathrm{i})dw_\mathrm{i} \end{aligned} \quad (12)$$

$$\begin{aligned} dT_\mathrm{m} =& \frac{1}{R_\mathrm{im}C_\mathrm{m}}(T_\mathrm{i} - T_\mathrm{m})dt \\ &+ (1 + Q_\mathrm{step}\sigma_\mathrm{level})\exp(\sigma_\mathrm{m})dw_\mathrm{m} \end{aligned} \quad (13)$$

$$\begin{aligned} dT_\mathrm{e} =& \frac{1}{R_\mathrm{ie}C_\mathrm{e}}(T_\mathrm{i} - T_\mathrm{e})dt + \frac{1}{R_\mathrm{ea}C_\mathrm{e}}(T_\mathrm{a} - T_\mathrm{e})dt \\ &+ (1 + Q_\mathrm{step}\sigma_\mathrm{level})\exp(\sigma_\mathrm{e})dw_\mathrm{e} \end{aligned} \quad (14)$$

and the output equation (which makes the system continuous-discrete, i.e. discretely observed):

$$Y_\mathrm{k} = T_\mathrm{i,k} + \exp(e_k) \quad (15)$$

Now the parameters of the full model can be listed:

C_i - Heat capacity of the interior $[\frac{kWh}{K}]$
C_e - Heat capacity of the envelope $[\frac{kWh}{K}]$
C_m - Heat capacity of the medium $[\frac{kWh}{K}]$
R_ie - Thermal resistance, interior to envelope $[\frac{K}{kW}]$
R_ea - Thermal resistance, envelope to ambient $[\frac{K}{kW}]$
R_im - Thermal resistance, interior to medium $[\frac{K}{kW}]$
A_w - Equivalent window area $[m^2]$
σ_i - Wiener process variance for state T_i $[Kh]$

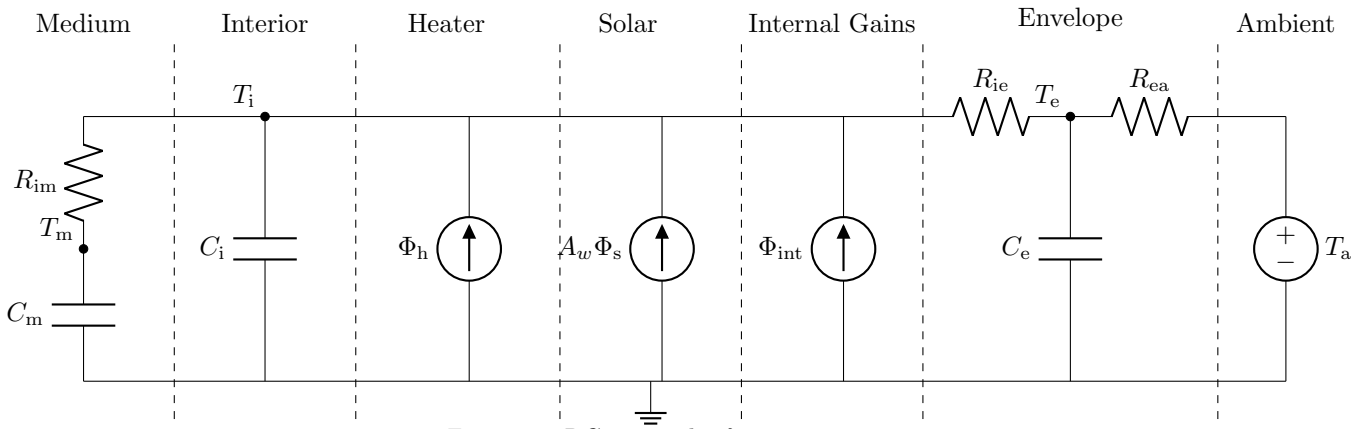

Figure 3: RC-network of $T_iT_eT_m\sigma$.

σ_e - Wiener process variance for state T_e $[Kh]$

σ_m - Wiener process variance for state T_h $[Kh]$

σ_level - Parameter for input-dependant variance [-]

the states:

T_i - Interior temperature $[°C]$

T_e - Envelope temperature $[°C]$

T_m - Medium temperature $[°C]$

and the inputs:

ϕ_h - Controlled heating input $[kW]$

ϕ_int - Internal heat gains $[kW]$

ϕ_s - Global solar radiation $[\frac{kW}{m^2}]$

T_a - Ambient temperature $[°C]$

Q_step - Heater input lag [-]

In this work, we will deal with the models $T_\mathrm{i}T_\mathrm{e}T_\mathrm{m}\sigma$, $T_\mathrm{i}T_\mathrm{e}\sigma$, $T_\mathrm{i}T_\mathrm{e}T_\mathrm{m}$ and $T_\mathrm{i}T_\mathrm{e}$, sorted in decreasing complexity. A model can be reduced by simply dropping a state, i.e. setting all the parameters associated with the state to 0 (as is the case from $T_\mathrm{i}T_\mathrm{e}T_\mathrm{m}\sigma$ to $T_\mathrm{i}T_\mathrm{e}\sigma$), or by setting the parameter denoted in the model name to 0 (as is the case from $T_\mathrm{i}T_\mathrm{e}T_\mathrm{m}\sigma$ to $T_\mathrm{i}T_\mathrm{e}T_\mathrm{m}$). We aim to estimate all of the parameters listed above, in addition to the initial states $\boldsymbol{x}_0 = [T_{\mathrm{i}0}, T_{\mathrm{m}0}, T_{\mathrm{e}0}]^T$, which together yields the full set of parameters $\boldsymbol{\theta}$.

Algorithm

To enable automated estimation of several model structures across many datasets, a simple heuristic on top of the algorithm outlined in equations 1-8 has been developed. Let the notation $A[]$ represent an associative array (i.e. hash map, dictionary, key-value pair).

Algorithm 1 summarizes the main steps of the procedure. A dataset $d \in \mathcal{D}$ refers to exactly one yearly dataset of PRBS-operation for one of the eight possible configurations (as depicted in figure 2). $\mathcal{M}$ refers to the set of months, and taking $d_m \leftarrow d[m]$ for a given m implies extracting the training data (i.e. PRBS-data) for that month. $\mathcal{S}$ refers to the set of model structures to consider, which is limited in this work to the set $\{T_\mathrm{i}T_\mathrm{e}T_\mathrm{m}\sigma, T_\mathrm{i}T_\mathrm{e}\sigma, T_\mathrm{i}T_\mathrm{e}T_\mathrm{m}, T_\mathrm{i}T_\mathrm{e}\}$. Let the CTSM-R algorithm, outlined by equations 1-8, be represented by the procedure named "est". The error named "StateCovError" implies that the state covariance matrix of the Kalman filter, $\boldsymbol{P}^i_{k|k-1}$ has ceased to become positive definite for some set of parameters $\boldsymbol{\theta}_i$, where k is the time step in the evolution of the states and i is the iteration in the CTSM-R algorithm. This is an irrecoverable error in the estimation procedure, as it makes further evolutions of the Kalman filter impossible, and a new parameter trajectory must be generated for the parameter search. This is done here by simply incrementing the initial

Algorithm 1 Estimation heuristic

Require: $\mathcal{D}$, $\mathcal{M}$, $\mathcal{S}$, $\boldsymbol{\theta}_0$, $\boldsymbol{\theta}_{max}$, $\boldsymbol{\theta}_{min}$, b

Initialize $c \leftarrow A[]$
for each $d \in \mathcal{D}$ **do**
  $c[d] \leftarrow A[]$
  for each $s \in \mathcal{S}$ **do**
    $c[d][s] \leftarrow A[]$
    for each $m \in \mathcal{M}$ **do**
      $d_m^{train} \leftarrow d[m]$
      $f \leftarrow A[]$
      repeat
        try
          $f \leftarrow \mathrm{est}(m', d_m, \boldsymbol{\theta}_0, \boldsymbol{\theta}_{max}, \boldsymbol{\theta}_{min})$
        catch StateCovError
          $n \leftarrow \mathrm{num\_states}(s)$
          $\boldsymbol{\theta}_0[\sigma_n^0] \leftarrow \boldsymbol{\theta}[\sigma_n^0] + 1$
        catch BoundsError
          $\boldsymbol{\theta}_{max} \leftarrow \boldsymbol{\theta}_{max} + b\boldsymbol{\theta}_{max}$
          $\boldsymbol{\theta}_{min} \leftarrow \boldsymbol{\theta}_{min} - b\boldsymbol{\theta}_{min}$
        end try
      until convergence **or** $\sigma_n^0 \geq 10$
      Reset $\boldsymbol{\theta}_0, \boldsymbol{\theta}_{max}, \boldsymbol{\theta}_{min}$
      $c[d][s][m] \leftarrow f$
    end for
  end for
end for

Ensure: Model is suitable, validate

value of the variance of the n^{th} state, where we assume that the number of states n of a model structure s can be retrieved with the procedure "num_states". The error "BoundsError" indicates that a minimum or maximum value in $\boldsymbol{\theta}_{min}, \boldsymbol{\theta}_{max}$ was hit for some parameter in the quasi-Newton method, and is handled by subtracting and adding those, respectively, by a multiplier b of themselves. The end result of the algorithm is a tree-like structure c, where each leaf node is a fit (model) f, or the empty array $A[]$ in the case of no convergence.

Results

As indicated by algorithm 1, an attempt is made to find a fit for each model structure, for each month, for each dataset (archetype). Due to the scope of this procedure, the presentation of the results w.r.t statistical analysis and simulation performance is limited to one archetype (AB03, variant 2) and model structure (the full model, $T_\mathrm{i}T_\mathrm{e}T_\mathrm{m}\sigma$), with the assurance that the procedure yields similar results for all datasets (archetypes), albeit with increased time constants and decreased UA-values as the building standard increases. Note that when referring to the *measurement* in the following, we are actually talking about an average of simulated zone-level temperatures.

Statistical validation

First, we analyze the residuals of the one-step predictions for the training data, $\boldsymbol{\epsilon}_k^{train}$, ref equation 7. Figure 4 shows the cumulative periodogram (CP) of these residuals on a per month basis, where the dotted red line represents the 95 % confidence-level for the assumption of white-noise on the residuals (uncorrelated, zero expectation and finite variance), which can be interpreted as the 95 % confidence-level that the model estimated describes the dynamics found in the training data sufficiently. The x-axis is a multiplier of the sampling frequency (with $0.5T_s$, or the Nyquist frequency, as the highest value, as frequencies above this limit are aliased), whereas the y-axis represents the accumulated normalized spectral density of the signal.

As can be seen from the figure, most of the periodograms satisfy the white-noise assumption. The ones that do not (for the models identified in January, July and November) bend slightly above the upper confidence limit, which points toward an abundance of low-frequency signals in the residuals. Hence, the white-noise assumption on the residuals does not hold, and there is room for improvement (i.e. more complex or differently formulated models) in the model selection. Because the violation of the white noise assumption occurs at low frequencies, a more complex treatment of the solar gains ϕ_s is a likely path to improvements. Measures to achieve this could be e.g. splining the solar input and making the solar gain input to the model a linear combination of the splines, or making the process noise in the interior state T_i dependent on the solar input. This is left for further work.

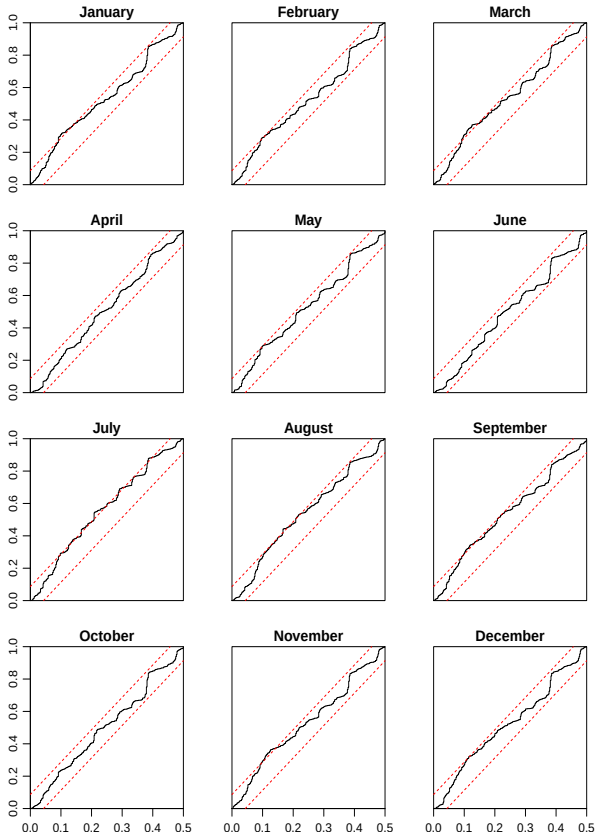

Figure 4: Cumulative periodogram for models $T_iT_eT_m\sigma$, $\forall m \in \mathcal{M}$.

Simulation performance

An important validation measure is simulation performance, i.e. conditioning the states on only the initial input x_0 for a given validation dataset $\mathcal{Y}_N^{val}$, which yields

$$\hat{\boldsymbol{Y}}_{N|0} = [y_0, \hat{y}_{1|0}, ..., \hat{y}_{k-1|0}, \hat{y}_{k|0}, ..., \hat{y}_{N|0}] \qquad (16)$$

where $\hat{y}_{k|0}$ instead of $\hat{x}_{k|0}$ is taken as the model prediction to include the measurement noise in equation 15. The reasoning behind testing simulation performance instead of one-step ahead prediction performance, is that the former implies the latter, while the converse not necessarily is the case (Coninck et al., 2016). Hence, testing for simulation performance ensures greater applicability, as they then can be used for load-forecasting and large-scale flexibility studies (Institute for Energy Technology, SINTEF, Norwegian University of Science and Technology , 2020).

The simulation performance for the models identified with the structure $T_\mathrm{i}T_\mathrm{e}T_\mathrm{m}\sigma_\mathrm{level}$ is shown in figure 5, plotted together with the 95% prediction interval (± 1.96SD), with

$$\mathrm{SD}_k = \mathrm{SD}(\hat{\boldsymbol{x}}_{k|0}) + \mathrm{SD}(\hat{\boldsymbol{y}}_{k|0}) = \sqrt{\boldsymbol{P}_{k|0}} + \sqrt{\boldsymbol{R}_{k|0}} \quad (17)$$

where $\boldsymbol{P}_{k|0}$ is the covariance matrix of the states at time $t = t_k$ conditioned on x_0, and $\boldsymbol{R}_{k|0}$ represents the measurement uncertainty. From the plot, it can be seen that the grey-box models are able to emulate the dynamics of the IDA-ICE models in a wide range of operating conditions. Starting with January, we see that the (grey-box) model is able to capture a steep increase in T_i (after a prolonged heater turn-off in PRBS-mode), with only a slight steady-state error in the days following. Furthermore, the prediction interval is quite narrow, indicating that the uncertainty associated with the model estimate is relatively low. For the model identified in February, the performance looks similar, although the steady-state error here is barely visible until Feb 27^{th}, where it increases to 0.5-1.0 °C. However, we see that this error is "picked up" by the prediction interval widening towards the end of the simulation period. The March and April

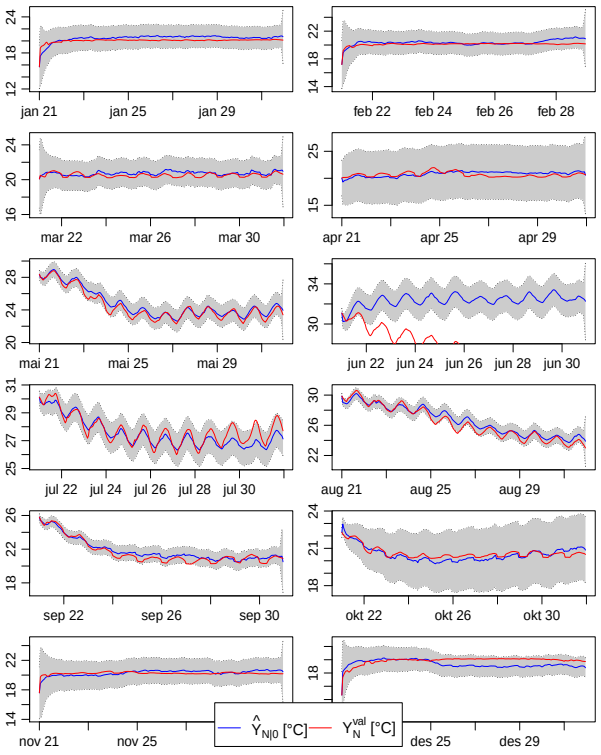

Figure 5: Simulation of T_i, $T_iT_eT_m\sigma$, $\forall m \in \mathcal{M}$. $\hat{Y}_{N|0}$ is the grey-box prediction, Y_N^{val} is the simulated/true value.

models show more irregularities, which (as with the CP of the residuals) could be caused by the model of the solar gains being too simple, with one parameter representing the equivalent area A_w. Again the deviation is captured by a widening of the prediction interval. The models from May, July, and August show good simulation performance, capturing wave-like behavior of the temperature, caused by the strong solar components in these months. The more irregular behaviour of the September and October models, similar to March and April, is also captured by the models. The only model that fails entirely at tracking the true temperature $\mathcal{Y}_N^{val}$ is the June model, where it appears to be a problem with a biased energy balance on one or more of the states (i.e. non-physical parameters).

Parameter consistency

Since the full model $T_\mathrm{i}T_\mathrm{e}T_\mathrm{m}\sigma$ is non-linear only in the process noise terms, we can summarize the dynamics by extracting the time constants $\boldsymbol{\tau} = [\tau_i, \tau_m, \tau_e]$. Furthermore, to look at the steady-state heat transfer from the building to the ambient, the UA-value (corresponding to the inverse of the equivalent resistance of the circuit in figure 3 from T_i to T_a, i.e. heat transfer coefficient with unit $\frac{W}{m^2K}$) is calculated.

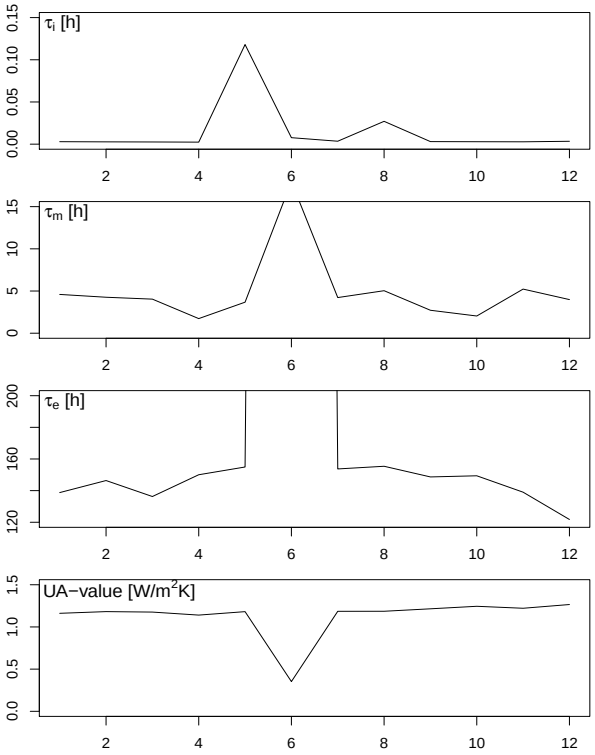

Figure 6: Time constants/UA, $T_iT_eT_m\sigma$, $\forall m \in \mathcal{M}$.

As can be seen from figure 6, the abstracted physical properties of the models show a good degree of consistency. The only exception is the June model (6), which explains the sub-par simulation performance of that model, ref figure 5. Although it is not visible in the plot, the time constant of the envelope τ_e goes above 3000 hours, which is a clear disconnect from building physics. At the same time, a drop in the otherwise stable UA-value can be seen, down from 1.2 to 0.5 $\frac{W}{m^2K}$, which is another reason to be distrust the model.

Discussion

The results show that it is possible to estimate models for all of the months. A full evaluation of the most suitable month for estimation is outside the scope

of this work, however, the failure of the June model hints at the summer months perhaps being less than ideal, as the difference between the indoor and ambient temperature is at its lowest. Even though this problem is bypassed to a certain degree in this work (since we are applying PRBS-signals in the identification period anyway), it is still apparent when looking at the time constant τ_e. This time constant exhibits a seasonal pattern, with larger values in the summer months than in the winter months. The other time constants shown in figure 6 do not show such seasonality, however, they have a less clear physical interpretation, since they are prone to "moving towards" or "moving from" the envelope, i.e. embedding more or less of the envelope thermal mass from one identification attempt to another. A natural step forward in assessing the best month for validation (which is relevant for the commissioning phase of future building MPC systems) would be to cross-validate the models, i.e. testing the simulation performance of a model identified in a certain month against all other months. Furthermore, the failure of the June model reinforces the findings in (Coninck et al., 2016), namely that models with non-physical parameters (τ_e in this case) are best avoided.

One possible approach to the problem of time-varying parameters in the context of MPC is to employ Moving Horizon Estimation (MHE) of parameters and states (Haseltine and Rawlings, 2005), (Maree et al., 2021), i.e. doing state and parameter estimation as a joint optimization problem. The models (and the procedure in general) identified in this paper can then serve as "initial" models for the MHE-problem, in addition to providing sensible upper and lower bounds for the parameters. Informally, one could say that MHE is a way of mathematically determining the optimal model given the conditions in the N preceding timesteps. On convergence failure in the MHE problem, one could e.g. revert back to the model from the previous timestep. In addition, some of the points mentioned in the discussion above could be formalized into heuristics, to avoid ending up with non-physical models, e.g. by checking the time constants and UA-value of the model after estimation. Furthermore, a subset of the parameters can be estimated instead of the whole model: in the case of $T_\mathrm{i}T_\mathrm{e}T_\mathrm{m}\sigma$, this could mean e.g. only estimating the capacitance C_e and A_w.

Some comments on the alternative formulation in equation 11 are warranted. First, the effect of the choice $\boldsymbol{u}'$ with a lag on the heating ϕ_h will have a very limited effect on the simulation performance, since no feedback to the model in the form of a measurement $\boldsymbol{y}_k$ is provided. The effect of $\boldsymbol{u}'$ lies in increasing the state covariance matrix $\boldsymbol{P}_{k|k-1}$ in the timesteps we are unsure about the evolution of the states (i.e. when rapid switching takes place), thereby increasing the Kalman gain $\boldsymbol{K}_k$ and putting more faith in the measurement $\boldsymbol{y}_k$. It is obvious that without updating, this has no effect, since $\hat{\boldsymbol{y}}_{k|k} = \hat{\boldsymbol{y}}_{k|k-1}$. Furthermore, the choice of limit for $|\Delta\phi_\mathrm{h}|_k = |\phi_{\mathrm{h},k} - \phi_{\mathrm{h},k-1}|$ will depend on the case at hand, e.g. a limit of 10 kW would be too high if an attempt was made to model a single apartment.

Finally, it should be mentioned that the procedure outlined in this work has been attempted on simulation data with normal operation. This did not yield satisfactory results, and implies that a PRBS-signal is needed for the procedure to work. However, since the conceived application is batch *offline* model generation using simulation models, we do not consider this to be a significant shortcoming.

Conclusion

An assortment of grey-box models have been identified and validated on a monthly basis (using the system identification software CTSM-R). The datasets used for the identification stem from IDA-ICE simulation models of Norwegian archetype blocks, which have been validated in a separate procedure. It has been shown that relatively simple model structures can capture the aggregated dynamics of the simulation models, by allowing the variance of the process noise to take on greater values in the time steps following rapid switching events. The simulation performance of the models is shown to be sufficient, as they are able to capture the dynamics of unseen data in a wide range of operating conditions, in addition to the true values falling mostly within the 95 % prediction interval of the models. Furthermore, the parameters with a physical interpretation exhibit a large degree of consistency across months, in addition to being relatively close to simple *a priori* calculations based on actual physical properties (ref. (Standards Norway, 2020)). A possible application of the models identified in this work could be as the starting point for Moving Horizon Estimation of states and parameters in a real-time MPC application, or as "simulators" (simulation models) in large-scale flexibility studies, where it is infeasible to use full simulation models.

Acknowledgment

This paper has been written within the Research Centre on Zero Emission Neighbourhoods in Smart Cities (FME ZEN), grant nr. 257660, and within the research project Flexbuild - "The value of end-use flexibility in the future Norwegian energy system", grant nr. 294920. The authors gratefully acknowledge the support from both the ZEN and Flexbuild partners, as well as the Research Council of Norway. Additionally, the authors gratefully acknowledge internal funding from SINTEF in connection with a company-wide initiative towards digitalization ("Konsernsatsing Digitalisering"), received through a Proof of Concept on MPC in buildings.

References

Bacher, P. and H. Madsen (2011). Identifying suitable models for the heat dynamics of buildings. *Energy & Buildings 43*, 1511–1522.

Bagle, M., H. T. Walnum, and I. Sartori (2020). Identifying grey-box models of Norwegian apartment block archetypes. In *BuildSim Nordic 2020*, pp. 293–300.

Blum, D. H., K. Arendt, L. Rivalin, M. A. Piette, M. Wetter, and C. T. Veje (2019). Practical factors of envelope model setup and their effects on the performance of model predictive control for building heating, ventilating, and air conditioning systems. *Applied Energy 236*, 410–425.

Bottolfsen, H. L., K. H. Andersen, J. Clauß, and I. Sartori (2020). Datasets for grey-box model identification from representative archetypes of apartment blocks in Norway . In *BuildSim Nordic 2020*, pp. 301–307.

Cígler, J., D. Gyalistras, J. Široky, V. Tiet, and L. Ferkl (2013). Beyond theory: the challenge of implementing model predictive control in buildings. In *Proceedings of 11th Rehva world congress, Clima*, Volume 250.

Coninck, R. D., F. Magnusson, J. Åkesson, and L. Helsen (2016). Toolbox for development and validation of grey-box building models for forecasting and control. *Journal of Building Performance Simulation 9*(3), 288–303.

Drgoňa, J., J. Arroyo, I. C. Figueroa, D. Blum, K. Arendt, D. Kim, E. P. Ollé, J. Oravec, M. Wetter, D. L. Vrabie, et al. (2020). All you need to know about model predictive control for buildings. *Annual Reviews in Control*.

European Commission (2019). Energy performance of buildings directive, Energy. `https://ec.europa.eu/energy/topics/energy-efficiency/energy-efficient-buildings/energy-performance-buildings-directive`.

Haseltine, E. L. and J. B. Rawlings (2005). Critical evaluation of extended Kalman filtering and moving-horizon estimation. *Industrial and Engineering Chemistry Research 44*(8), 2451–2460.

Institute for Energy Technology, SINTEF, Norwegian University of Science and Technology (2020). *Flexbuild Annual Report 1. Technical report with results analysis.*

Junker, R. G., A. G. Azar, R. A. Lopes, K. B. Lindberg, G. Reynders, R. Relan, and H. Madsen (2018, sep). Characterizing the energy flexibility of buildings and districts. *Applied Energy 225*, 175–182.

Kalamees, T. (2004). IDA-ICE: the simulation tool for making the whole building energy- and HAM analysis.

Kristensen, N. R. and H. Madsen (2003). *Continuous time stochastic modelling - Math Guite.*

Majdalani, N., D. Aelenei, R. A. Lopes, and C. A. S. Silva (2020, oct). The potential of energy flexibility of space heating and cooling in Portugal. *Utilities Policy 66*, 101086.

Maree, J., S. Gross, and H. T. Walnum (2021). Closed-loop system identification and control for demand response in buildings. Rotterdam (NL), 29 June - 2 July 2021.

Qin, S. J. and T. A. Badgwell (2003). A survey of industrial model predictive control technology. *Control engineering practice 11*(7), 733–764.

Renné, D. (2016). Resource assessment and site selection for solar heating and cooling systems. In R. Wang and T. Ge (Eds), *Advances in Solar Heating and Cooling*, pp. 13 – 41. Woodhead Publishing.

Romanchenko, D., J. Kensby, M. Odenberger, and F. Johnsson (2018). Thermal energy storage in district heating: Centralised storage vs. storage in thermal inertia of buildings. *Energy Conversion and Management 162*(February), 26–38.

Research Centre on Zero Emission Neighbourhoods in Smart Cities (2018). *ZEN Report No. 8 - Possibilities for supplying Norwegian Apartment Blocks with 4^{th} Generation District Heating.*

Serale, G., M. Fiorentini, A. Capozzoli, D. Bernardini, and A. Bemporad (2018). Model predictive control (mpc) for enhancing building and hvac system energy efficiency: Problem formulation, applications and opportunities. *Energies 11*(3), 631.

Standards Norway (2020). *Energy performance of buildings — Calculation of energy needs and energy supply (SN-NSPEK 3031:2020).*

TABULA/EPISCOPE (2013). Residential building typology. `https://episcope.eu/building-typology/country/no/`. (Accessed on 04/16/2021).

UN (2020). Climate Change, United Nations Sustainable Development. `https://www.un.org/sustainabledevelopment/climate-change/`.